King Saud University

Journal of Saudi Chemical Society

www.ksu.edu.sa
www.sciencedirect.com

CrossMark

ORIGINAL ARTICLE

On different photodecomposition behaviors of rhodamine B on laponite and montmorillonite clay under visible light irradiation

Peng Wang *, Mingming Cheng, Zhonghai Zhang

Water Desalination and Reuse Center, Division of Biological and Environmental Science & Engineering, King Abdullah University of Science and Technology, Thuwal 23955-6900, Saudi Arabia

Abstract In this study, laponite and montmorillonite clays were found to be able to decompose rhodamine B upon visible light irradiation ($\lambda > 420$ nm). Very interestingly, it was found that rhodamine B on laponite underwent a stepwise N-deethylation and its decomposition was terminated once rhodamine 110, as a decomposition product, was formed, whereas the same phenomenon was not observed for rhodamine B on montmorillonite, whose decomposition involved chromophore destruction. Mechanistic study revealed that the different photodecomposition behaviors of rhodamine B on laponite and montmorillonite were attributed to the oxidation by different reactive oxygen species, with laponite involving $HO_2^{\cdot}/O_2^{\cdot-}$ while montmorillonite involving $\cdot OH$. It was also found that the degradation pathway of rhodamine B on laponite switched from N-deethylation to chromophore destruction when solution pH was changed from 7.0 to 3.0, which was attributed to a much higher fraction of $HO_2^{\cdot}$ relative to $O_2^{\cdot-}$ under pH 3.0 than under pH 7.0. Based on the results, a mechanism of rhodamine dye decomposition on clay under visible light was proposed, involving the clay as an electron acceptor, electron relay between the adsorbed dye molecules and oxygen molecules, and subsequent reactions between the generated dye radical cations and different reactive oxygen species. The results of this study shed light on how to best utilize visible light for organic pollutant degradation on clays within engineered treatment systems as well as on many of naturally occurring pollutant degradation processes in soils and air involving clay.

© 2013 King Saud University. Production and hosting by Elsevier B.V.
Open access under CC BY-NC-ND license.

1. Introduction

Clay has long been employed as catalysts, adsorbents, and host materials in many of industrial, agricultural, and environmental decontamination processes and many of the clay applications are based on clay-organic interactions [16,29,33,36]. Generally, organic molecules interact with clay surfaces via the following mechanisms: (1) electrostatic interaction of ionic

* Corresponding author. Tel.: +966 2 808 2380.
E-mail address: peng.wang@kaust.edu.sa (P. Wang).
Peer review under responsibility of King Saud University.

ELSEVIER | **Production and hosting by Elsevier**

organic species with charged clay surfaces; (2) complexation of organic species with clay surfaces; for example, the π electrons of the phenyl in dioxins react with Lewis acid sites on laponite surfaces to form π electron complexes [21]; (3) coordination of nonionic species, such as alcohols, ketones, pyridines, with exchangeable metallic ions on clay surfaces [33,29].

Dye molecules, especially rhodamine dyes, are among the most commonly utilized probe molecules in studying clay-organic interactions in aqueous solutions (Martínez et al., 2005; Martínez et al., 2006; [3]; 2006). Two-dimensional clay surface provides a rigid microenvironment for the dye molecules to adsorb. Adsorption is usually a prerequisite for a photochemical reaction of the organic dyes to occur with the clay as the adsorbed dye molecules self-assemble on the clay surfaces to form molecular aggregates, leading to a photon-responsive hybrid material [24,4]; [27]. Photoinduced electron transfer, involving the adsorbed molecules and the clay, is one of the most known initiation steps for the photochemical reaction of the adsorbed molecules to proceed. For example, UV irradiation induced guest-to-host electron transfer and subsequent catalytic oxidation of pyrene [19,18,34], thianthrene [21], dioxin [21], and biphenyl [21] have been reported on laponite.

In most cases, clays act as electron acceptors during the electron transfer processes. It is known that the external surface of clay is built up of outer surface and lateral surface (i.e., edges). For example, the outer surface of laponite involves siloxane bonds while its lateral surface includes broken and terminated Si–O, Mg–O and/or Li–O bonds. These exposed structural metal cations at the edges are electron-deficient or Lewis acid sites, which are generally recognized as electron acceptors [19,25,5,31]. Following an electron transfer from the adsorbed organic molecules to the acceptor sites on the clays, organic radical cations are thus generated. It is believed that the ionic and high polarity nature of the clay surfaces stabilizes the formation and increases the yield of these radicals [12], making the clays ideal materials for photochemical studies.

In some other cases, clays may serve as electron donors during an electron transfer. For example oxygen lone pair in Si–O–Al of smectite is able to donate one electron to the excited methyl viologen (MV^{2+}) to form $MV^{\cdot+}$ [13]. Similar process has been reported to lead to a photodegradation of decabromodiphenyl ether [2].

UV-induced organic molecule decomposition on clay has been widely examined so far, but there has been little investigation on visible light induced organic decomposition [20,1,26], especially on the decomposition behaviors of organic dyes on clay surfaces. Since dye molecules adsorbed on clay can be potentially excited by visible light irradiation [39], an electron transfer between the adsorbed dye molecules and the electron acceptor sites on the clay surfaces might lead to a charge separation and subsequent formation of dye radical cations. It is thus expected that the formed dye radical cations can undergo hydrolysis or reactions with active oxygen species (e.g., $HO_2^{\cdot}$, $O_2^{\cdot-}$, $^{\cdot}OH$) present within the system, which may lead to a decomposition of the dye. As UV accounts for only less than 5% while visible irradiation makes up 50% of the total solar energy [40], investigation of visible irradiation assisted photodecomposition of dyes on clay is much needed as it will shed light on how to best utilize visible light for organic pollutant

degradation on clays within engineered treatment systems as well as on many of naturally occurring pollutant degradation processes in soils [14,15] and air [35] involving clay.

The objectives of this study are (1) to explore the visible light photodecomposition chemistry of rhodamine B on two clays, laponite and montmorillonite, which represent synthetic clays with a high purity and natural ones with such impurities as iron, respectively; (2) to propose and discuss the mechanism of rhodamine dye photodecomposition on clay under visible irradiation.

2. Experimental section

2.1. Materials and reagents

Montmorillonite, with a cation exchange capacity (CEC) of 100 meq/100 g, was purchased from Sigma–Aldrich (Montmorillonite K10) and treated as previously reported to remove metal impurities [32]. The as-obtained Na-montmorillonite (hereafter MMT) had a structural Fe content of 2.05% as determined by Inductively Coupled Plasma-Atomic Emission Spectroscopy (ICP-AES). Laponite, with a CEC of 55 meq/100 g, was supplied by Fernz Specialty Chemicals, Australia. Na-saponite (JCSS-3501, Kunimine Industry Co. Ltd.) was purchased from Clay Science Society of Japan. CEC of the saponite is 100 meq/100 g. Both laponite and saponite are synthetic materials (diffuse reflectance UV–vis spectra are presented in Figure S1). The main advantage of using these synthetic clays is that they are available in a high degree of purity and contain essentially no other active metal atoms such as Fe^{3+} and Cu^{2+}. Barnstead UltraPure water (18.3 MΩ) was used throughout the study. Horseradish peroxidase (POD) used for H_2O_2 measurement was purchased from the Huamei Biologic Engineering Co. (Luoyang, Henan, China) and the N,N-diethyl-p-phenylenediamine (DPD) reagent was from Merck (Whitehouse Station, NJ, USA).

Three rhodamine dyes were selected as the model compounds. Rhodamine B chloride (RB), rhodamine 110 chloride (R110), and rhodamine 123 chloride (R123) were purchased from Sigma–Aldrich. The structural formulas of the dyes are presented in Fig. 1. The type of amino and carboxyl groups determines the net molecule charge and thus plays a role in the interaction between the dye molecules and the clay surfaces. Known pKa values for the dyes are: RB 3.7, R110 4.3, and R123 6.1 (pKa value of R19 is not available in the literature. Due to the similarity of the structure to RB and R110, the pKa of R19 is estimated to be in the range 3.0–5.0.). Thus, at neutral pH, R123 is cationic while RB, and R110 form zwitterions due to the deprotonation of the carboxyl groups.

2.2. Photoreactor and light source

The visible irradiation source was a 500 W halogen lamp (Philip) positioned inside a cylindrical Pyrex flask, which was surrounded by a circulating water jacket to cool the lamp. A cut off filter was placed outside the water jacket to remove wavelengths below 420 nm to ensure a complete visible light irradiation. A schematic illustration of the photoreactor is presented in Figure S2. The photon flux of the 500 W halogen lamp at 560 nm was 3.4×10^{-8} einstein s^{-1}.
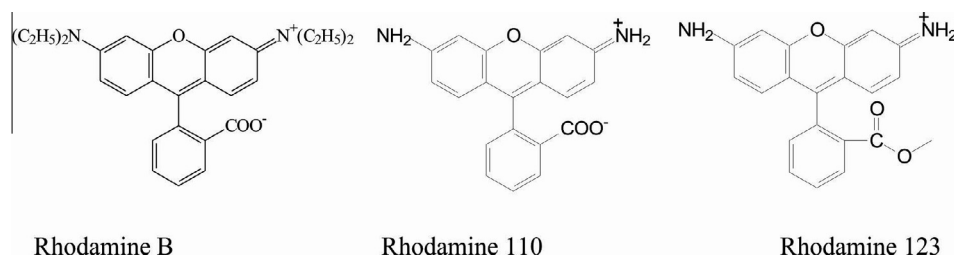
Figure 1   Structural formulas of rhodamine dyes.

2.3. Experimental and analytical procedures

Unless otherwise noted, all irradiation experiments were carried out in a cylindrical Pyrex vessel (60 mL) at an initial pH of 7.0. Typically, an aliquot of 5.0 mg of the clay was magnetically mixed with 50 mL of the dye solution with an initial concentration of 2×10^{-5} M. Prior to the irradiation experiments, the dye–clay suspension was mixed for up to 8 h to reach the dye adsorption equilibrium, which was confirmed by intermittent measurements of UV–vis absorption spectra of the centrifuged aqueous solution. The amount of the dye adsorbed was determined by the dye mass difference in the initial and equilibrium aqueous solutions. It should be noted that the dye molecules did not aggregate under the current dye/clay ratio and mixing time, which was confirmed by absorption measurements. Samples were collected at various reaction times and then centrifuged and filtered through a Millipore filter (pore size 0.22 μm). The UV–vis absorption spectra were measured with a Hitachi U-3010 spectrophotometer periodically to determine the photodecomposition kinetics and products. In all cases, the solution pH did not show any significant change before and after dye photodecomposition.

The dye photodecomposition products were also analyzed on a Shimadzu high performance liquid chromatography (HPLC) system (LC-20AT pump and UV–vis SPD-20A detector) equipped with a DIKMA Platisil ODS C-18 column (250×4.6 mm, 5 μm film thickness). For the mobile phase preparation, a mixture of $CH_3CN : H_2O = 1 : 1$ by volume was adjusted to pH 3.3 by H_3PO_4/PO_4^{3-}, $H_3PO_4 = 20$ mM. An Agilent 6310 Ion-Trap LC–MS with Electrospray Ion Source (EIS) was also used to identify the dye decomposition products. A GC–MS analysis was obtained on a Trio-2000 apparatus (Micromass UK Ltd.) equipped with a BPX70 column (size 30 m × 0.25 mm). Hydrogen peroxide generated was analyzed photometrically by the POD-catalyzed oxidation product of DPD at λ 551 nm ($\varepsilon = 21000$ M^{-1} cm^{-1}) [8].

3. Results and discussions

3.1. Decomposition of RB

3.1.1. Decomposition of RB on laponite

RB was adsorbed onto laponite and the amount of RB adsorbed was 0.05 mmol/g at pH 7.0. It was found that an aqueous RB solution in the absence of the clay underwent no decomposition within 10 h under visible irradiation, neither did RB in the clay suspension in the dark, implying both dye adsorption onto the clay and visible light irradiation are indispensable for the dye photodecomposition reaction to occur

(Under the experimental conditions, RB was stable and showed no blank reaction under visible irradiation. In the meantime, dark reactions of RB/clay suspension were not observed).

Fig. 2 presents the temporal UV–vis spectra changes of RB in laponite suspension, showing that RB was decomposed on laponite under visible irradiation. The most significant characteristics of the RB decomposition are that (1) the characteristic absorption peak of RB in laponite suspension underwent stepwise hypsochromic shifts and (2) the RB decomposition was terminated when the absorption peak moved to 502 nm. The hypsochromic shifts of the absorption peaks were found to result from the formation of a series of RB N-deethylated products in a stepwise manner.

Figs. 3 and Fig. 4 present the results of HPLC and LC–MS analyses of the RB decomposition intermediates and products. As shown in the HPLC chromatograph (Fig. 3), besides RB, five main products (I through V) showed up, whose relative abundance changed with time. These products were identified by positive ion EIS mass spectra to be the one-by-one N-deethylated RB decomposition products (Fig. 4). Table 1 presents a detailed identification of RB decomposition intermediates and products based on UV–vis, HPLC and LC–MS results. The UV–vis absorption peak at 502 nm corresponds to the fully N-deethylated RB, which is R110, while the absorption peaks at 541, 527, 531, and 514 nm correspond to RB decomposition products with a loss of one ethyl, two ethyls from one single nitrogen, one ethyl from each nitrogen (two ethyls combined), and three ethyls from two nitrogen combined, respectively. Fig. 3 clearly depicts the temporal process: over 90% of RB was decomposed within the first 60 min with a
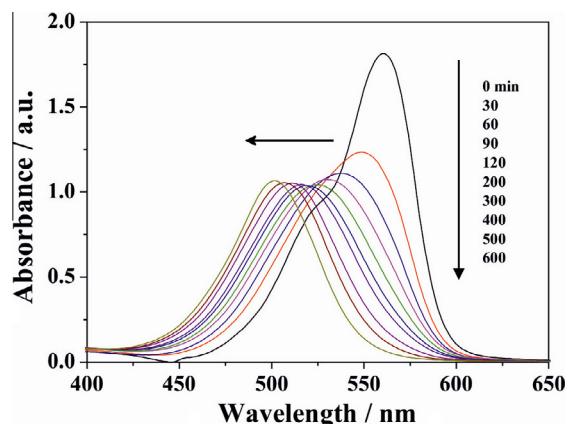

Figure 2   The temporal UV–vis spectra changes of RB in laponite suspension under visible irradiation.
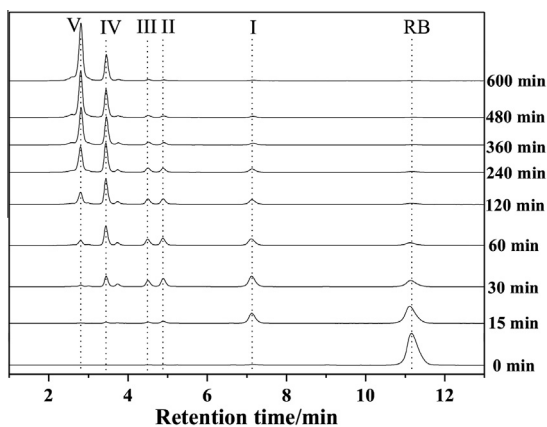
Figure 3 HPLC spectra of RB photodecomposition intermediates and products on laponite at various reaction times.

pseudo-first-order rate constant $k = 5.14 \times 10^{-2} \, min^{-1}$; the intermediates from I to IV were generated first but were subsequently consumed to produce the ultimate product V, which corresponds well with Fig. 2. Similar dealkylation phenomena, for example, the photooxidative N-deethylation of SRB in the DBS/P-25 system [17] and N-deethylation of RB in the TiO$_2$/SiO$_2$ [7] and NaBiO$_3$ [38] system under visible light irradiation, have been reported for non-clay systems.

To confirm the visible light induced decomposition of RB on laponite, another synthetic clay with a high degree of

purity, saponite, was also tested for RB decomposition under otherwise same conditions. The amount of RB adsorbed onto saponite was 0.03 mmol/g. Exactly the same N-deethylation behaviors as laponite were observed on saponite (Figure S3), that is, the reaction was terminated at R110. The yield of R110 was 69% in 1000 min.

Since RB N-deethylation was apparently in a stepwise manner, there must be a fast dynamic adsorption/desorption equilibrium of RB and its deethylated species between the bulk solution and the clay particle surfaces during the reaction. Understanding the interactions of these deethylated species with laponite will enable us to better understand the N-deethylation process. The type of amino groups of the dyes plays a significant role in forming effective electrostatic interaction with the clay surface. It is believed that RB is anchored on the clay surface through the $=N^+(CH_3CH_2)_2$ group via cation exchange. Since the inductive effect of the ethyl group would stabilize the positive charge at the nitrogen atoms, the more the alkyl groups, the more stable are the quaternary ammonium cations. Thus, as the N-deethylation process goes on, the intensity of the electrostatic attraction between RB decomposition intermediates (i.e., products I through V) and the lattice charge of the clay decreases. Therefore, it follows that the strength of the interaction of RB and its decomposition intermediates and products with laponite decreases in the order of RB > I > II > III > IV > V. Among all the intermediates and products, the fully N-deethylated one (V), R110, has the weakest interaction with laponite. As RB photodecomposition goes on, products I through IV are formed
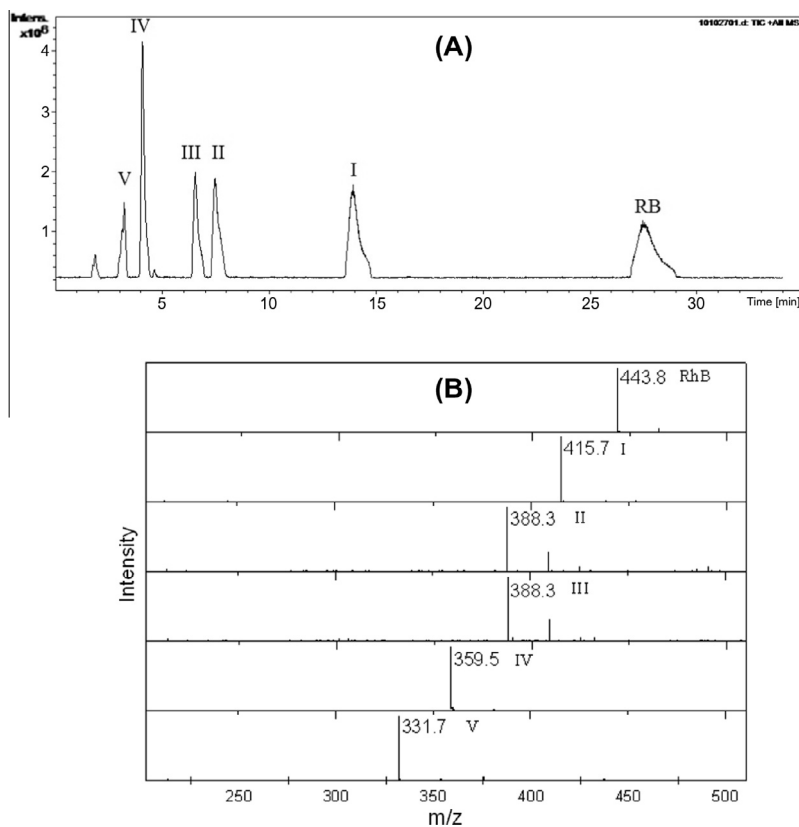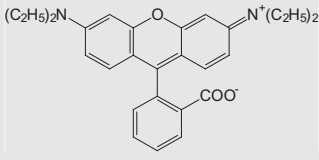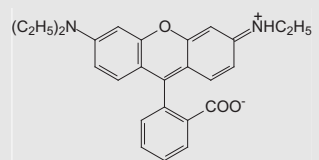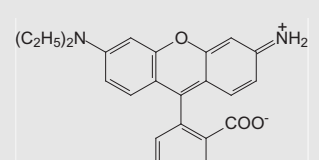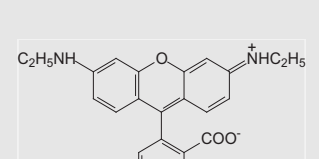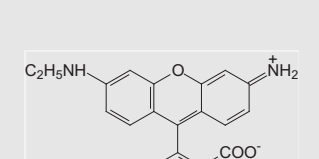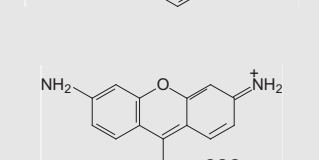

Figure 4 LC (A) and positive ion ESI mass spectra (B) of RB decomposition intermediates and products at 120 min of visible irradiation.

Table 1 Identification of RB decomposition intermediates and products by HPLC and LC-MS.

HPLC peaks	Maximum absorption (nm)	m/z	Corresponding intermediates	Structural formulas
RB	556	443.8	Rhodamine B	
I	541	415.7	N,N-diethyl-N'-ethylrhodamine	
II	527	388.3	N,N-diethylrhodamine	
III	531	388.3	N-ethyl-N'-ethylrhodamine	
IV	514	359.5	N-ethylrhodamine	
V	502	331.7	Rhodamine 110	

sequentially but later are all converted to R110 (V). As to be presented and discussed later, R110 was not decomposed on laponite, MMT and saponite at pH 7.0 as well as pH 3.0. Thus, RB decomposition stops where R110 is formed. A detailed RB decomposition mechanism is presented later in 'dye photodecomposition mechanism discussion' section.

3.1.2. Decomposition of RB on MMT

Unlike RB decomposition on laponite, RB decomposition on MMT showed no sign of termination at R110. The amount of RB adsorbed was 0.34 mmol/g in this case. MMT is chemically different from laponite in that it contains 2.05% of structural Fe impurity. Fig. 5 shows the temporal UV–vis spectra changes of RB in MMT suspension under visible irradiation. Clearly, under otherwise same conditions, RB in MMT suspension showed a hypsochromic shift of UV–vis absorption peak similar to that of RB in laponite, but the absorption intensity decreased monotonically with time, which stands in a sharp contrast with RB in laponite suspension. Moreover, the UV–vis absorption spectra revealed no new intermediates or products formed that would have manifested new absorp-
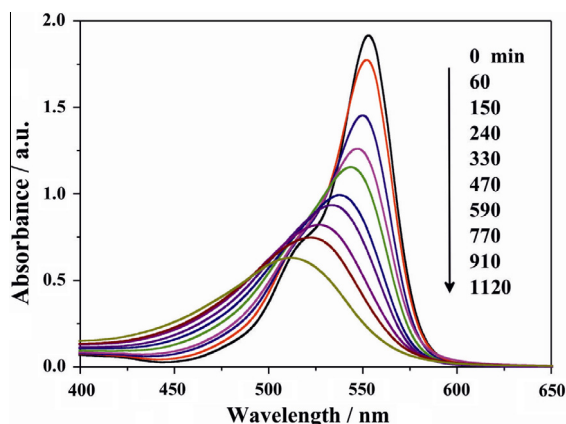
Figure 5 The temporal UV–vis spectra changes of RB in MMT suspension.

Figure 6 Kinetic plots of RB and R110 concentration as a function of reaction time in MMT (A) and laponite (B) suspensions.

tion features in the visible and near-ultraviolet region, indicating cleavage of the RB chromophore ring structure.

Fig. 6 presents kinetic plots of RB decomposition and R110 formation in the suspension of MMT (A) and laponite (B). As can be seen, 90% of RB was decomposed within 900 min in MMT suspension (pseudo-first-order rate constant $k = 1.60 \times 10^{-3}$ min^{-1}), but R110 concentration did not experience a significant change within the same timeframe. The maximum R110 yield was only 11% for RB in MMT within 900 min, which is much smaller than the maximum R110 yield for RB in laponite suspension within 600 min (ca. 60%) (Fig. 6B). The dramatic difference in R110 formation kinetics during RB decomposition illustrates the different decomposition behaviors of RB on laponite and MMT.

RB photodecomposition on laponite, saponite, and MMT indicates that the two-dimensional clay surface provides a suitable microenvironment for the dye decomposition reactions to take place possibly driven by certain oxidants. Since oxygen was present in all of the testing systems, O_2 and/or other relevant active oxygen species might be responsible for RB decomposition. Moreover, different RB decomposition behaviors with different clays imply that, different oxidizing species are involved with different clays in terms of RB decomposition, which will be discussed later in detail.

3.2. Decomposition of other rhodamine dyes

Since R110 is the ultimate product of RB decomposition by laponite and saponite and also a minor product of RB decomposition by MMT, R110 decomposition was studied to better understand RB decomposition behaviors on these clays. Adsorption of R110 was 0, 0.02, and 0.09 mmol/g at pH 7.0 on laponite, saponite, and MMT, respectively. Experimental results showed that no R110 decomposition was observed on any clay within 10 h of visible irradiation, which agrees well with the termination of RB decomposition on laponite and saponite when it proceeds to R110. A possible interpretation of R110's resistance to -decomposition will be discussed in the mechanism section.

R123, a rhodamine dye with an ester group at the carboxy-phenyl moiety in place of the carboxyl group in R110, was also tested under otherwise same conditions. The ester group of R123 behaves differently from the carboxyl group in R110 in
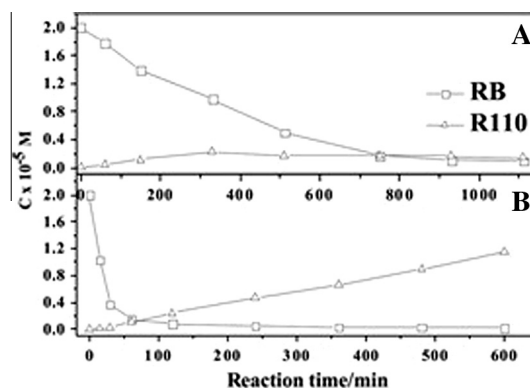
that it does not deprotonate to be negatively charged, so R123 is cationic, regardless of solution pH. Compared with the zero adsorption of R110 on laponite at pH = 7.0, the amount of R123 adsorbed was 0.07 mmol/g on laponite. Figure S4 presents the temporal UV–vis spectra changes of R123 in laponite suspension, indicating a significant R123 decomposition (38% decomposition in 8 h).

3.3. pH effect on RB decomposition

Protonation of carboxyl groups can be achieved at a low pH, which changes the net chemical charges of zwitterionic dye molecules. At pH 3.0, more than 83% of RB molecules are protonated according to calculation and thus RB-laponite interactions are expected to be much stronger at pH 3.0 than at neutral pH, which is partially evidenced by a substantial increase in the amount of adsorbed RB on laponite (0.44 mmol/g at pH = 3.0 versus 0.05 mmol/g at pH 7.0). As shown in Fig. 7, at pH = 3.0, a significant decrease in the UV–vis absorption intensity accompanied with slight hypsochromic shifts of the peaks of RB in laponite was clear, implying a chromophore destruction. As a matter of fact, RB almost completely faded at the end of 450 min at pH = 3.0, which is quite different from RB in laponite at pH 7.0 (Fig. 2). Chromophore destruction of RB in laponite at pH = 3.0 was further verified by a GC–MS analysis of the products (Table S1). The major products identified were organic acids, such as acetic acid, oxalic acid, butanedioic acid, benzoic acid, and phthalic acid, all of which were the chromophore cleavage and further RB degradation products.

Since R110 decomposition by laponite was not observed at pH = 3.0, RB decomposition must not proceed to R110 (R110 aqueous solution underwent slight decomposition at neutral pH (5% conversion in 600 min, see SI) and very slow decomposition at pH 3.0 (11% conversion in 400 min) under visible irradiation). Thus we can conclude that RB decomposition on laponite at pH = 3.0 changes from N-deethylation being the only process at pH = 7.0 to chromophore destruction being dominant. When N-deethylation is the only process, the reaction terminates when RB is fully N-deethylated. If chromophore destruction dominates over N-deethylation, the reaction continues until RB completely fades. The pH dependent RB photodecomposition behaviors have been reported
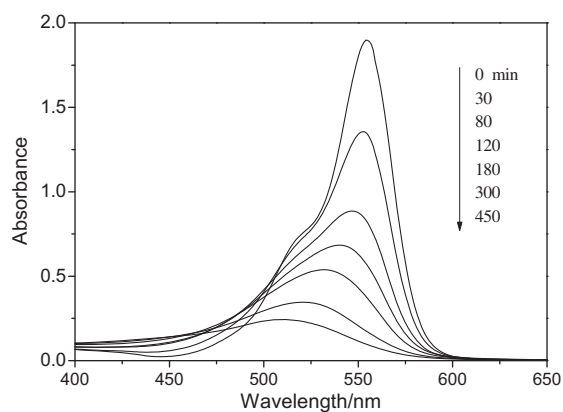
Figure 7 The temporal UV–vis spectra changes of RB in laponite suspension at pH 3.0 under otherwise same conditions.

in a $Pb_3Nb_4O_{13}$ photocatalytic system [22], where the pH effect was interpreted in terms of different RB adsorption modes on the catalyst surface under different pHs.

3.4. Dye photodecomposition mechanism discussion

The objective of this section is to come up with a plausible mechanism to explain the following observations about different but interesting RB decompositions under visible illumination: (1) RB undergoes N-deethylation on laponite and saponite at pH 7.0 and its decomposition terminates at R110, whereas, under pH 3.0, RB decomposition undergoes a more powerful chromophore destruction; (2) RB is decomposed on MMT at both pH 7.0 and 3.0 and its decomposition at both pHs undergoes chromophore destruction; (3) R110 does not decompose on any clay under both pH 3.0 and 7.0. Tests were conducted to confirm some key points of the proposal mechanism.

First, a number of trials were conducted in an attempt to find out the reactive oxygen species involved in the reactions. Isopropyl alcohol, a strong ·OH radical scavenger, at a concentration of 2 mM, was added to RB in clay suspensions to see if it has some influence on RB photodecomposition. It turned out that the RB reaction in laponite suspension was not at all affected, while RB decomposition in MMT suspension was much suppressed by isopropyl alcohol. As shown in Figure S5, RB decomposition by MMT was only 25% in 600 min in the presence of isopropyl alcohol compared with 82% in its absence. The results indicate that no ·OH radicals were involved during RB decomposition by laponite under visible irradiation while they were possibly the major reactive species responsible for RB decomposition by MMT.

Moreover, the results show that 37 μM of H_2O_2 were generated in RB in laponite suspension at pH 7.0 in 7 h, indicating a possible involvement of superoxide radical anions ($O_2^{·-}$) and its hydrolysis product hydroperoxyl radical ($HO_2^·$). This is so because, as is generally known, superoxide radical anion spontaneously dismutes to O_2 and hydrogen peroxide quite rapidly ($8.6 \times 10^5 \text{ M}^{-1} \text{ s}^{-1}$ at pH 7.0) [6] and reduction of $HO_2^·/O_2^{·-}$ by organics also produces H_2O_2. Furthermore, a photochemical formation of H_2O_2 involving electron transfer to O_2 to form $O_2^{·-}$ radical has been proposed on a number of metal (e.g.,

TiO_2, ZnO) and nonmetal oxide (e.g., clay) surfaces [9,30,28]. To further confirm the involvement of $O_2^{·-}$, the effect of Cu^{2+} on the decomposition of RB with laponite was investigated at pH 7.0. The reaction of Cu^{2+} with $O_2^{·-}$ (Eq. (1)) is known to occur very rapidly. Considering that the reaction product: Cu^+, reacts with H_2O_2 in a Fenton-like reaction to produce hydroxyl radicals (·OH) [10], 2 mM isopropyl alcohol was added with 0.1 mM Cu^{2+} to exclude the influence of ·OH. As shown in Figure S6, the decomposition of RB on laponite in this case was greatly suppressed by Cu^{2+} and isopropyl alcohol. The RB decomposition in the presence of Cu^{2+} was only 4% as compared with 90% in 60 min in the absence of Cu^{2+} (Fig. 3). For the purpose of comparison, the influence of 0.1 mM Ca^{2+} was also tested on RB decomposition and the results showed that the presence of Ca^{2+} did not change RB decomposition at all (Figure S7). The significant suppression of RB decomposition by Cu^{2+} strongly supports the involvement of $O_2^{·-}$ as a main reactive intermediate.
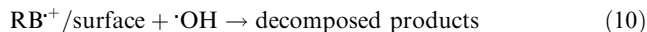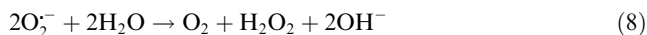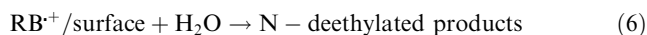
$$Cu^{2+} + O_2^{·-} \rightarrow Cu^+ + O_2 \qquad (1)$$
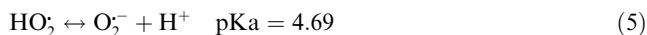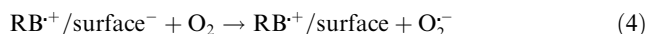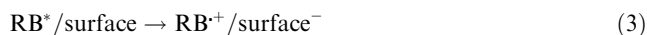
The yield of H_2O_2 in RB in MMT suspension was measured to be 9 μM in 10 h at pH 7.0, which provides a suitable source for ·OH. Montmorillonite clay usually contains a significant amount of iron species that are mainly located in the octahedral layers by substituting for the aluminum. [37] The MMT used in this study has an iron content of 2.05%, so in such a system, the iron from MMT reacts with H_2O_2 as Fenton agents to produce ·OH. Hydroxyl radicals are highly reactive and could induce a deep RB degradation, i.e., chromophore destruction. The use of iron-containing clays as heterogeneous Fenton reagents has been reported for organic pollutant degradation [9,11].

Based on all the above discussed and using RB as an example, our proposed reaction pathways for dye decomposition on clays under visible irradiation are listed in Eq. ((2)–(refspseqn11)). A detailed explanation is as follows. As demonstrated earlier, light irradiation is indispensable for the dye decomposition reaction to occur, so the photosensitization of dye molecules is an important step to initiate the reaction. Therefore, RB adsorption onto a clay surface is very important for such a photosensitization process since it permits the electron injection from the excited RB to the clay. In more detail, a RB molecule gets adsorbed onto a clay surface to form an adsorbed RB, which in turn absorbs visible light to enter its excited state (Eq. (2)); the excited RB molecule transfers one electron to a Lewis acid site at the clay edge surface with itself forming a dye radical cation (Eq. (3)). The Lewis acid site on the clay edge surface acts as a relay, which then transfers the electron to the surface of an adsorbed oxygen molecule to form $O_2^{·-}$ (Eq. (4)). Similar photo-induced clay-to-O_2 electron transfer has been reported to generate $O_2^{·-}$ radical [9].

Active oxygen species are mostly generated nearside the adsorption group of the dye (Eq. (4)) on the clay surface and thus much prefer to attack the positions of the dye that are near the clay surface. Since RB is anchored on the clay surface through its amino groups, the RB decomposition starts with a loss of its ethyl groups on the nitrogen (Eqs. (6), (7a), and (7b)). More specifically, the hydrolysis of the generated dye radical cation produces N-deethylated products (Eq. (6)) [7,30,11] and simultaneously, the dye radical cation reacts with $HO_2^·/O_2^{·-}$, leading to both N-deethylation (Eq. (7a)) and RB

further decomposition (Eq. (7b)). It has been reported that N-deethylation proceeds by forming a N-centered radical while destruction of chromophore structure proceeds by generation of a carbon-centered radical [7].

At pH 7.0 where $O_2^{\cdot-}$ is the major active oxygen species within RB in laponite suspension (Eq. (5)), only N-deethylation occurs on laponite according to our results, indicating the attack of $O_2^{\cdot-}$ at RB is highly selective. In an early paper, the same behavior was reported: RB was nearly 100% converted to R110 through N-deethylation at pH 6.0 ($95\%O_2^{\cdot-} + 5\%HO_2^{\cdot}$) in a CdS suspension under visible irradiation [37], and $O_2^{\cdot-}$ was proposed to be the reactive intermediate in this system. At pH 3.0 0 where $HO_2^{\cdot}$ now is the major active oxygen species, oxidation of RB by $HO_2^{\cdot}$ ($98\%HO_2^{\cdot} + 2\%O_2^{\cdot-}$) undergoes mainly chromophore destruction as the results showed earlier. The above can be further explained from the following two aspects. First, $HO_2^{\cdot}$ is more reactive and has a higher redox potential than $O_2^{\cdot-}$ [23]. The one electron reduction potential of $O_2^{\cdot-}$ and $HO_2^{\cdot}$ is $+0.89$ V vs. NHE and $+1.44$ V vs. NHE, respectively. Secondly, at a neutral pH, the negatively charged COO^- groups experience a stronger electrostatic repulsion from the clay surfaces and thus RB molecules are relatively farther from the clay surface generated active oxygen species (i.e., $O_2^{\cdot-}$) than at pH 3.0. Thus, $=N^+(CH_3CH_2)_2$ groups have a higher possibility to be attacked by $O_2^{\cdot-}$ than other portions of the molecules at pH 7.0 (Eq. (7a)). This argument is supported by the photodecomposition of R123, which has no carboxyl groups. Whereas, at pH 3.0, $HO_2^{\cdot}$ tends to attack both $=N^+(CH_3CH_2)_2$ group and the center carbon of the molecules (Eq. (7b)).

$$RB/surface + h\nu \rightarrow RB^*/surface \tag{2}$$

$$RB^*/surface \rightarrow RB^{\cdot+}/surface^- \tag{3}$$

$$RB^{\cdot+}/surface^- + O_2 \rightarrow RB^{\cdot+}/surface + O_2^{\cdot-} \tag{4}$$

$$HO_2^{\cdot} \leftrightarrow O_2^{\cdot-} + H^+ \quad pKa = 4.69 \tag{5}$$

$$RB^{\cdot+}/surface + H_2O \rightarrow N - deethylated\ products \tag{6}$$

$$RB^{\cdot+}/surface + O_2^{\cdot-} \rightarrow N - deethylated\ products \tag{7a}$$

$$RB^{\cdot+}/surface + HO_2^{\cdot} \rightarrow N - deethylated\ and\ products \tag{7b}$$

$$2O_2^{\cdot-} + 2H_2O \rightarrow O_2 + H_2O_2 + 2OH^- \tag{8}$$

$$\equiv Fe^{2+} + H_2O_2 \rightarrow \equiv Fe^{3+} + \cdot OH + OH^- \tag{9}$$

$$RB^{\cdot+}/surface + \cdot OH \rightarrow decomposed\ products \tag{10}$$

Note: $=Fe^{2+}$ denotes clay structural iron. To further probe the origin of $O_2^{\cdot-}$, the RB decomposition in laponite suspension was carried out in an O_2 free aqueous medium (i.e., oxygen-depleted by argon gas). In the absence of O_2, the RB decomposition was greatly suppressed with a much reduced deethylation rate as compared with the case in the presence of O_2 (Fig. 8), which agrees well with the proposed reaction pathway in Eqs. (4), (7a), and (7b) and serves as an evidence supporting the hypothesis that $HO_2^{\cdot}/O_2^{\cdot-}$ is the active oxygen species that is responsible for the deethylation and chromophore destruction.

With MMT, the presence of a significant amount of iron species causes the production of $\cdot OH$ (Eq. (8)), which is a much
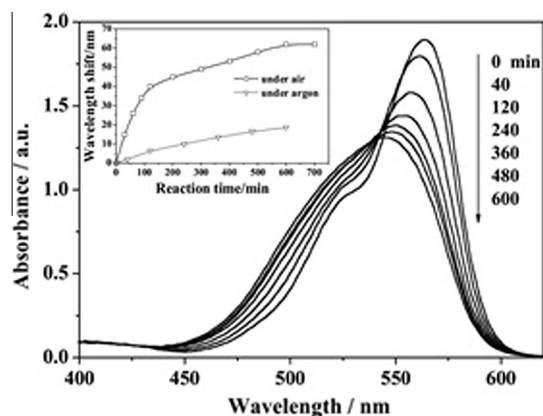

Figure 8 The temporal UV–vis spectra changes of RB in laponite suspension under an oxygen-depleted aqueous medium. Inset is a comparison of the wavelength shifts of the absorption peak of RB under argon and under air as a function of irradiation time.

more potent oxidizing species than $HO_2^{\cdot}/O_2^{\cdot-}$. The decomposition of RB through chromophore destruction in this case conforms to conventional Fenton reaction mechanisms (Eqs. (9) and (10)), which has been reported in numerous publications.

As to the result that R110 was not decomposed by any clay studied (laponite, saponite, and MMT) at either pH 3.0 or 7.0, one possible explanation is that the electron-donating energy level of the excited R110* relative to that of the clay electron accepting sites is not suitable, which makes the excited R110* not able to donate an electron to the clay surface and thus Eq. (2) cannot take place. As a result, neither dye radical cation nor superoxide radical anion is formed and R110 thus does not undergo any significant decomposition.

4. Conclusion

In summary, in this study, we found the RB decomposed on clays' visible illumination to varying degrees, depending on the types of the clays and solution pH. Very interestingly, different RB decomposition pathways were identified on different clays and a general mechanism of dye decomposition on clay under visible light was proposed to explain the results. The results of this study provide an insight to the underlying physicochemical mechanisms in heterogeneous systems based on clays.

5. Declaration of interest

The authors report no conflicts of interest. The authors alone are responsible for the content and writing of the paper.

Appendix A. Supplementary data

Supplementary data associated with this article can be found, in the online version, at http://dx.doi.org/10.1016/j.jscs.2013.11.006.

References

[1] A.J. Acher, I. Rosenthal, Wat. Res. 11 (1977) 557.
[2] M.Y. Ahn, T.R. Filley, C.T. Jafvert, L. Nies, I. Hua, J. Bezares-Cruz, Environ. Sci. Technol. 40 (2006) 215.
[3] J. Bujdák, N. Iyi, J. Phys. Chem. B 109 (2005) 4608.
[4] J. Bujdák, Appl. Clay Sci. 34 (2006) 58.
[5] A.G. Cairns-Smith, H. Hartman, Clay minerals and the origin of life, Cambridge University Press, 1987.
[6] C.C. Chen, W. Zhao, P.X. Lei, J.C. Zhao, N.B. Serpone, Chem. Eur. J. 10 (2004) 1956.
[7] F. Chen, J.C. Zhao, H. Hidaka, Int. J. Photoenergy 5 (2003) 209.
[8] M.M. Cheng, W.H. Ma, J. Li, Y.P. Huang, J.C. Zhao, Y.X. Wen, Y.M. Xu, Environ. Sci. Technol. 38 (2004) 1569.
[9] M.M. Cheng, W.J. Song, W.H. Ma, C.C. Cheng, J.C. Zhao, J. Lin, H.Y. Zhu, Appl. Catalysis B: Environ. 77 (2008) 355.
[10] M.K. Eberhardt, R. Colina, K. Soto, J. Org. Chem. 53 (1988) 1074.
[11] J. Feng, X. Hu, P. Yue, H. Zhu, G. Lu, Ind. Eng. Chem. Res. 42 (2003) 2058.
[12] E. Giannakopoulos, P. Stathi, K. Dimos, D. Gournis, Y. Sanakis, Y. Deligiannakis, Langmuir 22 (2006) 6863.
[13] N. Kakegawa, T. Kondo, M. Ogawa, Langmuir 19 (2003) 3578.
[14] T. Katagi, J. Agric. Food Chem. 39 (1991) 1351.
[15] L. Kong, J.L. Ferry, Environ. Sci. Technol. 37 (2003) 4894.
[16] P. Laszlo, Acc. Chem. Res. 19 (1986) 121.
[17] G. Liu, X. Li, J. Zhao, H. Hidaka, N. Serpone, Environ. Sci. Technol. 34 (2000) 3982.
[18] X.S. Liu, K.K. Lu, J.K. Thomas, Langmuir 8 (1992) 539.
[19] X.S. Liu, J.K. Thomas, Langmuir 7 (1991) 2808.
[20] D. Madhavan, K. Pitchumani, J. Photochem. Photobiol. A: Chem. 153 (2002) 205.
[21] Y. Mao, S. Pankasem, J.K. Thomas, Langmuir 9 (1993) 1504.
[22] O. Merka, V. Yarovyi, D.W. Bahnemann, M. Wark, J. Phys. Chem. C 115 (2011) 8014.
[23] A. Nadezhdin, H.B. Dunford, J. Phys. Chem. 83 (1979) 1957.
[24] M. Ogawa, K. Kuroda, Chem. Rev. 95 (1995) 399.
[25] S. Pankasem, J.K. Thomas, J. Phys. Chem. 95 (1991) 6990.
[26] B. Pączkowska, S. Strzelec, B. Jędrzejewska, L.Å. Linden, J. Pączkowski, Appl. Clay Sci. 25 (2004) 221.
[27] R.H.A. Ras, J. Németh, C.T. Johnston, E. DiMasi, I. Dékány, R.A. Schoonheydt, Phys. Chem. Chem. Phys. 6 (2004) 4174.
[28] Sawyer, D.T., Jr. Nanni, E.J., Jr. Roberts, J.L., 1982. Electrochemical and Spectrochemical Studies of Biological Redox Components, Chapter 24, p. 585.
[29] T. Shichi, K. Takagi, J. Photochem. Photobiol. C: Photochem. Rev. 1 (2000) 113.
[30] R. Shinozaki, T. Nakato, Microporous Mesoporous Mater. 113 (2008) 81.
[31] D.H. Solomon, Clays Clay Miner. 16 (1968) 31.
[32] W.J. Song, M.M. Cheng, J.H. Ma, W.H. Ma, C.C. Chen, J.C. Zhao, Environ. Sci. Technol. 40 (2006) 4782.
[33] B.K.G. Theng, The Chemistry of Clay-Organic Reactions, 1st ed., Adam Hilger, London, 1974, Chapter 5.
[34] J.K. Thomas, Chem. Rev. 105 (2005) 1683.
[35] C.R. Usher, A.E. Michel, V.H. Grassian, Chem. Rev. 103 (2003) 4883.
[36] P. Wang, A.A. Keller, Langmuir 25 (2009) 6856.
[37] T. Watanabe, T. Takizawa, K. Honda, J. Phys. Chem. 81 (1977) 1845.
[38] K. Yu, S.G. Yang, H. He, C. Sun, C.G. Gu, Y.M. Ju, J. Phys. Chem. A 113 (2009) 10024.
[39] Z.H. Zhang, Y.J. Yu, P. Wang, ACS Appl. Mater. Interfaces 4 (2012) 990.
[40] Z.H. Zhang, P. Wang, Energy Environ. Sci. 5 (2012) 6506.